Technical Note

Hydrodynamics of a Broad-Crested Weir with Rounded Edges

Sunhanut Chaokitka[1] and Hubert Chanson[2]

Abstract: A broad-crested weir is a flat-crested structure, acting as a hydraulic control, which may be used to measure the discharge. Detailed observations of free-surface profiles, pressure, velocity, and boundary shear stress distributions were performed in a large-sizes weir with rounded corners. The data highlighted a rapid redistribution of pressure and velocity profiles. The dimensionless discharge coefficients ranged from 0.92 to 1.04. The velocity data implied a developing boundary layer along the broad crest. The boundary shear stress increased as the flow accelerated toward the downstream end of the crest, where a local peak of shear stress was observed. The shear stress was relatively uniform across the weir, except next to the sidewalls. Based upon the nonhydrostatic pressure and nonuniform velocity distributions, the detailed hydrodynamic characterization demonstrated that the flow was critical along the entire broad crest length. **DOI: 10.1061/JIDEDH.IRENG-10666.**

Author keywords: Broad crest; Pressure; Velocity; Boundary shear stress; Physical modeling; Hydraulic structures.

Introduction

Hydraulic engineering encompasses the storage, regulation, and safe conveyance of water in natural and manufactured systems. Hydraulic structures play an essential role in water storage, flow control and measurements (Wegmann 1911; Jaeger 1956; Montes 1998). At a dam and weir, the spillway crest controls the discharge outflow for ungated structures [Fig. 1(a)]. The discharge above the crest is typically expressed by the weir equation (Henderson 1966)

$$Q = C_D \times \sqrt{g \times \left(\frac{2}{3} \times (H_1 - \Delta z)\right)^3} \times B \tag{1}$$

with Q = volume flow rate; C_D = dimensionless discharge coefficient; H_1 = upstream above crest, Δz = weir crest elevation; g = the gravity acceleration; and B = crest breadth [Fig. 1(b)]. The discharge coefficient C_D is a function of the weir shape, weir height, and upstream total head (Bos 1976; Ackers et al. 1978). For an ideal fluid overflow above a broad-crested weir, theoretical considerations yield: $C_D = 1$ (Henderson 1966; Chanson 2004).

A broad crest refers to as a flat crest for which the length along the flow direction L is significantly greater than the upstream head above the crest $(H_1 - \Delta z)$. Thus, the streamlines above the crest are parallel to the crest, i.e., straight horizontal, and yield near-hydrostatic pressure distributions (Bos 1976; Castro-Orgaz and Hager 2017). Fig. 1(a) presents a photograph of large dam spillway equipped with a broad crest. Physically, the crest is considered broad when the ratio $L/(H_1 - \Delta z)$ is larger than 1.5 to 3 (Govinda Rao and Muralidhar 1963). Although less efficient than an ogee crest, the broad crest design is simpler and facilitates vehicular access during and post construction. The hydraulics of broad-crested weirs has been investigated for nearly two centuries. Seminal contributions encompassed Bélanger (1841), Bazin (1896) and Woodburn (1932). Some systematic comparison showed larger discharge coefficients with an upstream crest rounding of the weir crest because of the reduction in flow separation (Tison 1950; Ramamurthy et al. 1988). Recent physical studies of broad crest on tall structures illustrated the effect of large vortical structures in the approach flow (Gonzalez and Chanson 2007; Zhang and Chanson 2016).

The present study aimed to characterize the pressure, velocity, and boundary shear stress distributions properties on a broad crest with rounded edges. The experimental observations were undertaken above a 1 m wide 1.4 m high structure. The data set provided a detailed characterization of the two-dimensional flow field.

Experimental Facility and Instrumentation

New experiments were conducted in a large flume with very smooth inflow conditions. The water was supplied by three alternating currents (AC) pumps through a manifold-style diffuser installed in a 1.7 m deep and 5 m wide intake basin, which was equipped with a series of baffles and flow straighteners. The flow smoothly converged in a 2.8 m long symmetrical section with a converging ratio 5.08:1, yielding a waveless flow into the flume. The flume was 0.985 m wide with acrylic sidewalls. The broad-crested weir was 0.542 m long (L = 0.542 m) with a PVC invert and rounded ends, with a 1.4 m high vertical upstream wall (Δz = 1.4 m). The upstream rounding radius was 0.058 m, and the downstream rounding radius was 0.012 m, with 180° bend, as sketched in Fig. 1(b). The broad-crested weir ended with a 1.4 m high steep stepped (1V:0.8H) chute.

The upstream water level was recorded with a point gauge using a MeasumaX single column digital height readout and with an accuracy ±0.05 mm. The water depth measurements along the crest were performed with three systems: a rail-mounted point gauge,

[1]Researcher, School of Civil Engineering, Univ. of Queensland, Brisbane, QLD 4072, Australia; presently, Structural Engineer, Aurecon, Brisbane, QLD 4006, Australia.

[2]Professor in Hydraulic Engineering, School of Civil Engineering, Univ. of Queensland, Brisbane, QLD 4072, Australia (corresponding author). ORCID: https://orcid.org/0000-0002-2016-9650. Email: h.chanson@uq.edu.au

Note. This manuscript was submitted on June 5, 2025; approved on September 2, 2025; published online on November 4, 2025. Discussion period open until April 4, 2026; separate discussions must be submitted for individual papers. This technical note is part of the ***Journal of Irrigation and Drainage Engineering***, © ASCE, ISSN 0733-9437.

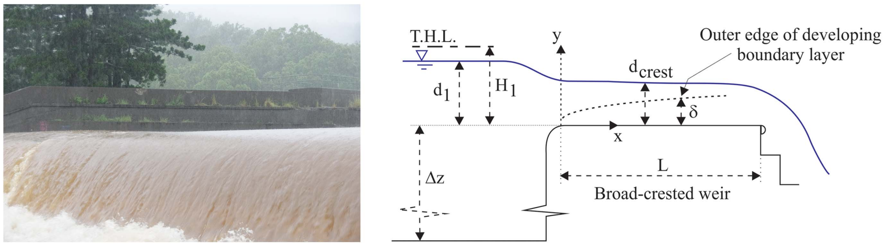

(a) (b)

Fig. 1. Flow with a broad crest: (a) Gold Creek Dam spillway (Australia) in operation on 26 February 2022 for $Q = 38\ m^3/s$; and (b) Definition sketch of an overflow above a broad crest with rounded edge.

a sidewall ruler and some sideview photography. The accuracy was ±0.5 mm. The pressure and velocity were measured using a 3.1 mm diameter stainless steel Dwyer series 160 Prandtl-Pitot tube. The tube featured a 1.19 mm diameter dynamic tapping and four 0.51 mm diameter static openings located 9 mm behind the dynamic tapping. The Prandtl-Pitot tube was connected to an air-water manometer open to the atmosphere. The position of the velocity probe was measured by a Mitutoyo digital scale unit with a vertical accuracy of ±0.025 mm, and the horizontal accuracy was ±1 mm. The local boundary shear stress τ_o was recorded with the Prandtl-Pitot tube lying on the invert acting as a Preston tube. Based upon the Prandtl mixing length theory, the boundary shear stress is related to the velocity reading V_b

$$\tau_o = \rho \times \left(\kappa \times \frac{V_b}{N}\right)^2 \tag{2}$$

with ρ = water density; κ = von Karman constant ($\kappa = 0.4$); and N = inverse of the velocity power law exponent, i.e., $N = 7$ for a smooth turbulent boundary layer (Cabonce et al. 2019). Photographic and video observations were recorded with an Apple iPhone Xs, a Casio EX-10 Exilim camera and a dSLR Pentax K-3 camera.

Visual observations were conducted for discharges up to $0.20\ m^3/s$. Velocity, pressure and boundary shear stress measurements were undertaken for upstream heads above crest $0.110\ m < (H_1 - \Delta z) < 0.235\ m$, corresponding to $0.20 < (H_1 - \Delta z)/L < 0.45$, and water discharges between $0.058\ m^3/s$ and $0.193\ m^3/s$ (Table 1). The experimental flow conditions are summarized in Table 1 and compared to previous physical studies of broad-crested weirs with rounded edge.

Basic Flow Properties

Flow Patterns

For all experiments (Table 1), the upstream flow was smooth and quiescent with very low inflow turbulence, as evidenced by dye injection. The water velocity increased over the broad crest and the flow became supercritical on the downstream steep slope. Fig. 2 illustrates a few typical flow conditions and two video movies are available in the digital appendix (Appendix I). Dye injection showed that the streamlines were nearly parallel to the invert about the middle section of the crest, while streamline curvature was observed at both upstream and downstream ends. The video movies CIMG8069.mov and CIMG8073.mov illustrate two different overflow conditions, in which the streamlines are highlighted by dye injection (Supplemental Materials). As the water flowed over the flat crest, the free-surface elevation gradually decreased. Herein, the downstream rounding forced the streamlines to turn downward toward the 1V:0.8H steep chute, as reported by Zhang and Chanson (2015) with a 1V:1H steep slope.

The longitudinal free surface profiles were recorded for several upstream heads above crest and typical data sets are reported in Fig. 3. The data highlighted a good agreement between the different

Table 1. Experimental flow conditions of broad-crested weir studies with rounded edges

Reference	B (m)	L (m)	Δz (m)	Weir geometry	Q (m^3/s)	Re	Comment
Present study	0.985	0.542	1.4	Rounded edges and vertical wall	0.001 to 0.2 0.058 to 0.193	0.4×10^5 to 8.1×10^5 2.4×10^5 to 7.8×10^5	Visual observations Velocity, pressure and boundary shear stress measurements
Woodburn (1932)	0.61	3.05 to 4.57	0.53	Rounded edge and vertical wall	0.057 to 0.311	3.7×10^5 to 20×10^5	
Isaacs (1981)	0.25	0.38	0.064	Rounded edge and vertical wall	0.0008 to 0.009	0.12×10^5 to 1.4×10^5	
Ramamurthy et al. (1988)	0.254	0.3048	0.1016	Rounded edge and vertical wall	—	—	
Gonzalez and Chanson (2007)	1.0	0.60	0.90	Rounded edge and vertical wall	0.046 to 0.18	1.8×10^5 to 7.2×10^5	Geometry 1
		0.88	0.99	Rounded edge and vertical wall	0.05 to 0.26	3.2×10^5 to 10×10^5	Geometry 2
		0.62	0.99	Rounded edge with overhanging	0.0064 to 0.17	2.7×10^5 to 6.8×10^5	Geometry 3
		0.62	0.99	Rounded edge and vertical wall	0.0064 to 0.21	2.7×10^5 to 8.4×10^5	Geometry 4
Felder and Chanson (2012)	0.52	1.01	1.0	Rounded edge and vertical wall	0.0025 to 0.142	1.9×10^5 to 11×10^5	
Zhang and Chanson (2016)	0.985	0.6	1.0	Rounded edge and vertical wall	0.035 to 0.20	1.4×10^5 to 8×10^5	

Note: B = channel breadth; L = broad-crest length; Q = water discharge; Re = Reynolds number defined in terms of the hydraulic diameter D_H; Δz = weir crest height; and (—) = information not available.

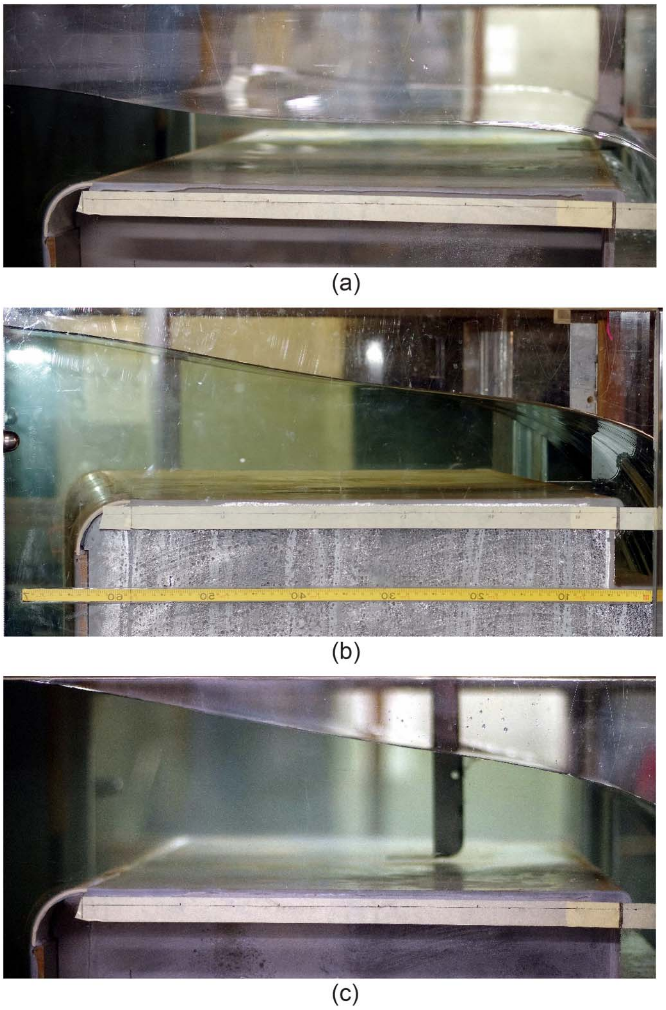

Fig. 2. Photographs of broad-crested weir overflow with flow direction from left to right—(a) $Q = 0.0585\ m^3/s$, $(H_1 - \Delta z)/L = 0.203$; (b) $Q = 0.149\ m^3/s$, $(H_1 - \Delta z)/L = 0.369$; and (c) $Q = 0.194\ m^3/s$, $(H_1 - \Delta z)/L = 0.435$.

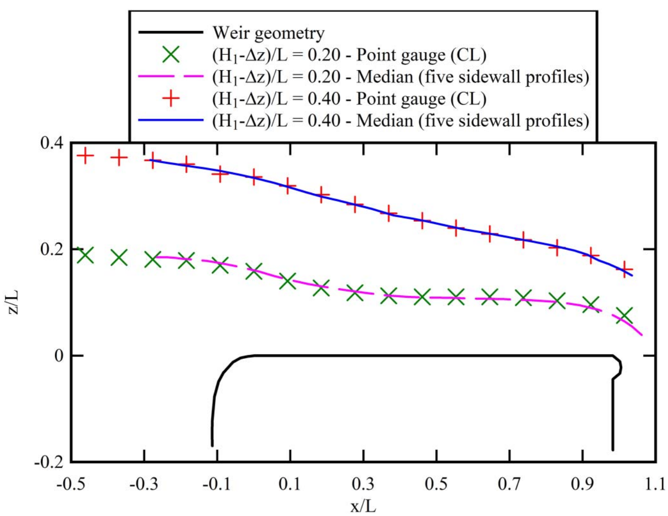

Fig. 3. Longitudinal free-surface profiles above the broad-crested weir: comparison between centerline point gauge data and sideview imaging data. (Median of five photographs.)

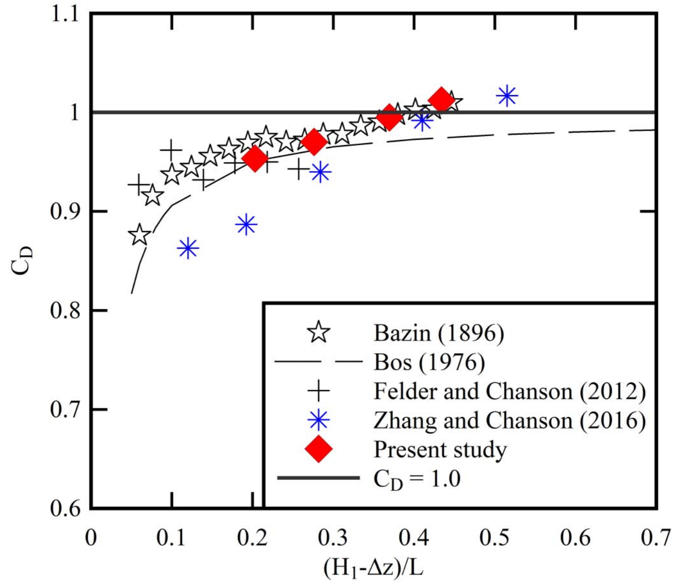

Fig. 4. Dimensionless discharge coefficient above broad-crested weirs with rounded edges—Comparison between present study and earlier data sets. (Bazin 1896, Bos 1976, Felder and Chanson 2012, Zhang and Chanson 2016.)

measurement techniques. While the water surface was flat in the middle of the crest, the curvature of the surface was relatively significant in the vicinity of both ends of the broad crest (Fig. 3). At low discharges, the water depth was relatively constant along the crest, before rapidly decreasing at the downstream end of the weir. At high discharges, in contrast, the flow was not parallel to the invert at any point along the length of the weir. These patterns were consistent with previous works (e.g., Zhang and Chanson 2016).

Discharge Coefficient

The dimensionless discharge coefficient C_D was derived from the measured head above crest $(H_1 - \Delta z)$ and the discharge calculated from the equation of conservation of mass

$$Q = \iint_A V_x \times dA \tag{3}$$

with the velocity measurements performed above the crest at $x/L = 0.55$. The discharge coefficient data were approximately a linear function, with increasing dimensionless discharge coefficient with increasing dimensionless upstream head $(H_1 - \Delta z)/L$ (Fig. 4)

$$C_D = 0.90 + 0.26 \times \frac{H_1 - \Delta x}{L} \quad \text{for } 0.2 < \frac{H_1 - \Delta x}{L} < 0.45 \tag{4}$$

The present data are compared to earlier data sets of broad-crested weirs with rounded edges in Fig. 4 (Bazin 1896; Bos 1976; Felder and Chanson 2012; Zhang and Chanson 2016). The comparison showed a good agreement, with C_D positively correlated to the dimensionless upstream head above the crest.

Fig. 5. Dimensionless distributions of pressure and velocity above the broad-crest centerline: (a) pressure distributions for $(H_1 - \Delta z)/L = 0.20$; and (b) velocity distributions for $(H_1 - \Delta z)/L = 0.20$.

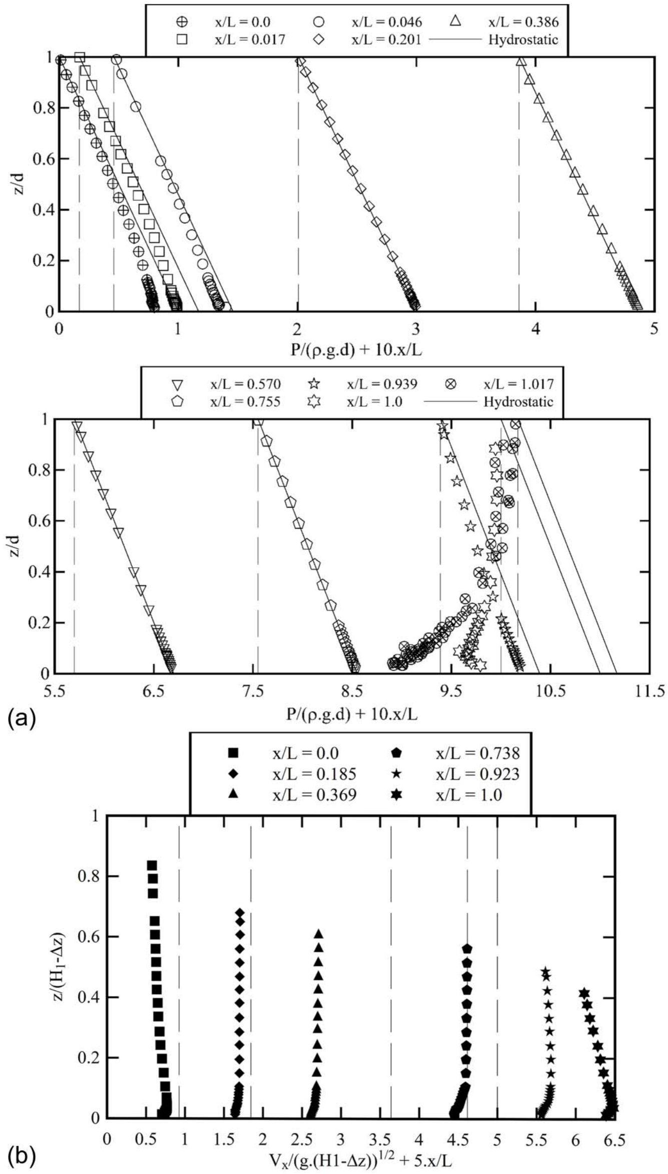

Velocity and Boundary Shear Stress

Pressure and Velocity Distributions

For all experiments, the data sets showed a longitudinal redistribution of the pressure field. The pressure distributions were nonhydrostatic at the upstream and downstream ends of the broad crest, and were hydrostatic only about the midsection of the weir crest. This is illustrated in Fig. 5(a), presenting typical vertical distributions of pressure.

The velocity data showed a major redistribution in velocity profiles from the upstream end toward downstream end of the broad crest [Fig. 5(b)]. For $0.185 < x/L < 0.74$, the velocity distributions presented a typical profile observed in an open channel flow, with zero at the invert and a monotonically increasing velocity toward the free surface. At the upstream and downstream ends of the broad crest, the velocity distributions markedly differed. The maximum velocity was observed about midwater column, as a direct consequence of the streamline curvature [Fig. 5(b)]. Along the crest, the longitudinal variations in velocity distributions implied the development of a turbulent boundary layer along the crest invert, as previously discussed (e.g., Gonzalez and Chanson 2007; Zhang and Chanson 2016).

Boundary Shear Stress

The boundary shear stress along the crest invert was measured with a Prandtl-Pitot tube acting as a Preston tube. The measured boundary shear stress ranged from 0.1 to 22 Pa. Typical data sets are presented in Fig. 6.

On the channel centerline, the boundary shear stress increased almost monotonically from the upstream end of the crest toward its downstream end. In the middle of the crest, the trend was nearly linear [Fig. 6(a)]. The rate of increase in shear stress was positively correlated to the dimensionless upstream head $(H_1 - \Delta z)/L$. A slightly different trend was observed at the lowest flow rate, i.e., $(H_1 - \Delta z)/L = 0.20$, with a nearly constant dimensionless shear stress. Overall, the dimensionless boundary shear stresses $\tau_o/[\rho \times g \times (H_1 - \Delta z)]$ ranged from 0.00003 to 0.01, corresponding to a Darcy-Weisbach friction factor from 0.001 to 0.3. The present data were close to the data sets of Felder and Chanson (2012) obtained using two different approaches, namely the momentum integral principle and the law of the wall next to the invert.

The boundary shear stress data were reasonably uniformly distributed across the breadth of the crest [Fig. 6(b)]. Some sidewall effects were observed with some local maximum in shear stress next to the walls, and these were about symmetrical on both sides. The local maximum in boundary shear stress was believed to be linked to the formation of elongated corner vortices with horizontal axis. Such vortical structures were likely an extension of the spiral vortices seen upstream of the vertical upstream wall of the weir by Rouse (1938, pp. 75 and 271) and Gonzalez and Chanson (2007, p. 109). A contour plot of boundary shear stress is illustrated in Fig. 6(b). The contour map showed the boundary shear effects imposed by the crest invert and sidewalls boundary of the wall as well as the rapid flow acceleration near the downstream end of the crest (i.e., $0.8 < x/L < 1$).

Critical Flow Conditions

At a spillway crest, the flow condition is critical because the specific energy is minimum (Bakhmeteff 1912, 1932; Henderson 1966). At a broad crest, the specific energy is minimum and the flow must be critical along the entire broad crest. For a frictionless free-surface flow, a detailed general solution of critical flow was developed, encompassing nonhydrostatic pressure and nonuniform velocity distribution situations. There exists an unique relationship between the pressure correction coefficient Λ, the velocity correction coefficient β, and the dimensionless discharge coefficient C_D (Appendix II). Combining with the equation of conservation of mass, the condition for minimum specific energy gives a relationship between the ratio $X = d/E_{min}$

$$X^3 - \frac{1}{\Lambda} \times X^2 + \frac{1}{2} \times \left(\frac{2}{3}\right)^3 \times \frac{\beta \times C_D^2}{\Lambda} = 0 \qquad (5)$$

in which d = expression of the critical depth for nonhydrostatic pressure distribution and nonuniform velocity distribution. While Eq. (5) presents four types of solution depending upon the sign of the discriminant (Chanson 2006), the present data

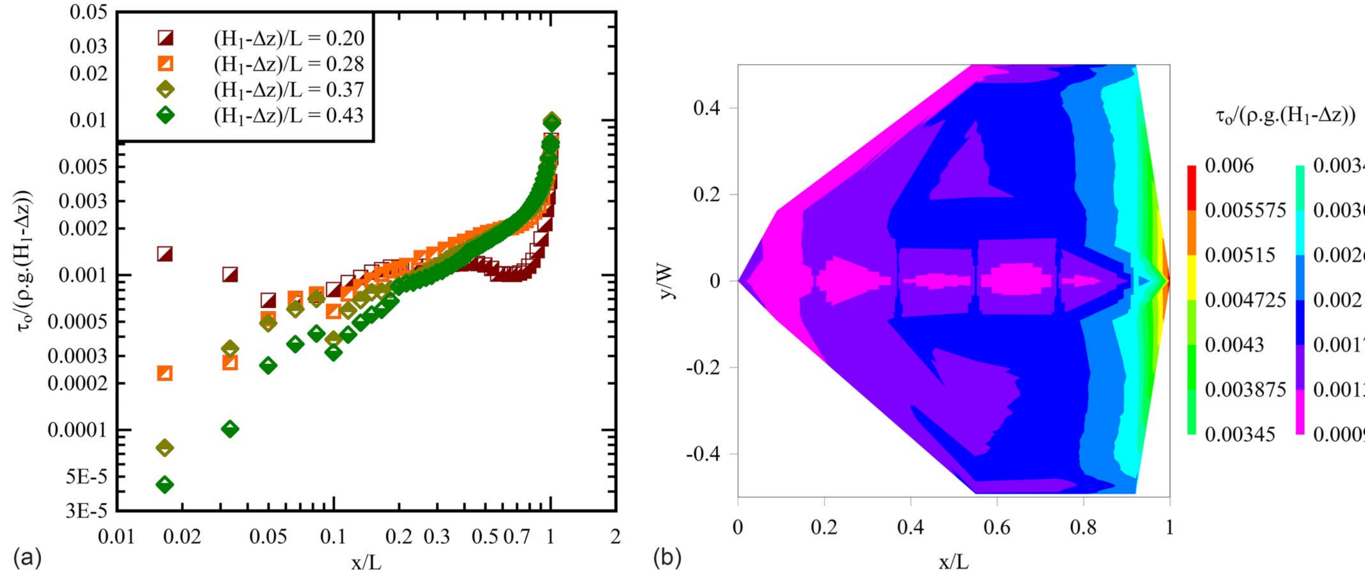

Fig. 6. Dimensionless boundary shear stress above the broad-crested weir: (a) longitudinal distributions of boundary shear stress above the broad-crest centerline; and (b) contour plot of dimensionless boundary shear stress above the broad-crest for $(H_1 - \Delta z)/L = 0.20$.

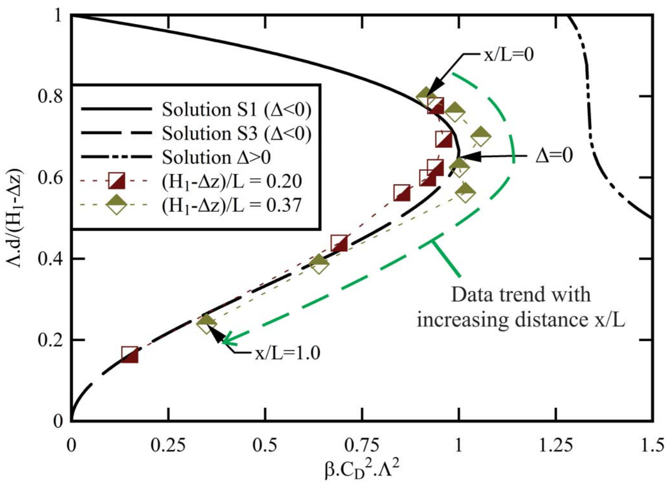

Fig. 7. Dimensionless flow depth above the crest $\Lambda \times d/(H_1 - \Delta z)$ as a function of $\beta \times C_D^2 \times \Lambda^2$ along the length of the crest—Comparison between data and theoretical solution [Eq. (5)] for $(H_1 - \Delta z)/L = 0.20$ and 0.37.

followed relatively closely two of the solutions, as previously reported. In Fig. 7, two complete data sets are shown. In the current study, the pressure and velocity correction coefficients Λ and β were derived from the pressure and velocity measurements respectively (Appendix III). The comparison between theoretical solution and experimental data indicated a change in solution depending upon the longitudinal location x/L as illustrated in Fig. 7.

Implicitly, the current experimental data demonstrated that the flow conditions were critical above the entire broad crest. It is acknowledged that the theoretical solution assumed no energy loss, while the present velocity data indicated the presence of a bottom boundary layer development. The latter implied some boundary friction, while the local shear stress maxima next to the sidewalls suggested some strong secondary motion in the bottom corners.

Conclusion

New experiments were undertaken with a focus on the flow field on a large broad crest with rounded edges. The fluid flow measurements encompassed free-surface, velocity, pressure, and boundary shear stress distributions. Although the data were overall in agreement with the detailed literature, they brought newer insights into the fluid flow motion.

The critical flow conditions took place along the whole streamwise length of the broad crest, although the velocity and pressure distributions were nonuniform and nonhydrostatic at the upstream and downstream ends. The marked deviations at both ends of the weir crest were caused by the rapid redistributions of flow field and streamline curvature. The longitudinal distributions of dimensionless boundary shear stresses on the crest centerline, corresponded to Darcy-Weisbach friction factors increasing from 0.001 to 0.3 with increasing streamwise distance. The dimensionless discharge coefficients ranged from 0.92 to 1.04, while the correction coefficients Λ and β varied within $0.3 < \Lambda < 1.01$ and $1.01 < \beta < 1.03$ above the crest. The transverse distributions of boundary shear stress were symmetrical about the crest centerline, with local maxima next to the sidewalls likely caused by elongated tornadolike eddies emanating from the bottom of the weir upstream wall.

The present data set was collected in a large-size facility, and the results can be extrapolated to full-scale prototypes with minimum scale effects. They showed that the dimensionless discharge coefficients for broad-crested weir with rounded edges increased with increasing upstream head above crest. The study highlighted the importance of the approach flow conditions and some implications for the three-dimensional flow motion over the weir crest, e.g., in terms of boundary shear stresses.

Appendix I. Video Movies of Broad-Crested Weir Overflow

New physical experiments were undertaken in a relatively large facility with very smooth inflow conditions. The broad-crested weir was 0.542 m long, 0.985 m wide with a PVC invert and rounded ends, with a 1.4 m high vertical upstream wall. Video movies were

Table 2. List of digital video movies and flow conditions

Geometry	$H_1 - \Delta z$ (m)	Q (m^3/s)	$(H_1 - \Delta z)/L$	Video movie filename	Camera (and lens)	Description
Present study	0.135	0.080	0.249	CIMG8069.mov	Casio EX-10 Exilim	HD movie [30 fps] with dye injection
	0.175	0.121	0.323	CIMG8073.mov	Casio EX-10 Exilim	HD movie [30 fps] with dye injection

Note: H_1 = upstream head; Q = discharge; and Δz = weir height.

recorded during some experiments with colored dye injection (see Supplemental Materials). Their description and the corresponding flow conditions are listed in Table 2.

Appendix II. Theoretical Considerations

The relationship between volumetric flow rate above a weir crest, upstream reservoir level, and weir crest geometry [Eq. (1)] is based upon a combination of the equation of conservation of mass, the Bernoulli principle applied between the upstream reservoir and weir crest, and the definition of critical flow conditions in open channels. For a rectangular hydraulic structure, the equation of conservation of mass states

$$Q = V_{crest} \times d_{crest} \times B \quad \text{Continuity principle} \tag{6}$$

with V_{crest} = cross-sectional averaged velocity at the crest, d_{crest} = water depth at the crest and B = transverse breadth of the crest. The Bernoulli principle applied between the upstream reservoir and weir crest yields

$$E_{crest} = H_1 - \Delta z \quad \text{Bernoulli principle} \tag{7}$$

with E_{crest} = specific energy at the crest and Δz = weir crest elevation above the reservoir invert [Fig. 1(b)]. In open channels, it is common to use the depth-averaged specific energy within the frame of relevant assumptions (Liggett 1993; Chanson 2006; Castro-Orgaz and Chanson 2014)

$$E = \Lambda \times d + \beta \frac{V^2}{2 \times g} \tag{8}$$

with Λ and β = pressure and velocity correction coefficients, respectively, defined as

$$\Lambda = \frac{1}{2} + \int_0^d \frac{P}{\rho \times g \times d} \times dy \quad \text{pressure correction coefficient} \tag{9}$$

$$\beta = \frac{\int_0^d V_x \times V_x \times dy}{d \times V^2} \quad \text{velocity correction coefficient} \tag{10}$$

where P = local water pressure; y = distance normal to the invert; and V_x = local velocity component. Physically, the coefficients Λ and β respectively account for the nonhydrostatic pressure and nonuniform velocity distribution at the weir crest. For a hydrostatic pressure distribution, $\Lambda = 1$, and $\beta = 1$ for an uniform velocity distribution. At the weir crest, critical flow conditions occur and E is minimum (Bakhmeteff 1912, 1932; Chanson 2004)

$$\left(\frac{\partial E}{\partial d} = 0\right)_{Q=\text{constant}} \quad \text{Critical flow conditions} \tag{11}$$

Thus, the following relationship holds at the weir crest:

$$\Lambda - \beta \times \frac{q^2}{g \times d_{crest}^3} = 0 \quad \text{Critical flow conditions} \tag{12}$$

assuming that $\partial\Lambda/\partial d = 0$ and $\partial\beta/\partial d = 0$, with q the unit discharge: $q = Q/B$. Eq. (B-7) satisfies the minimum specific energy condition for smooth, frictionless flows with nonuniform velocity profile and nonhydrostatic pressure distribution (Chanson 2006).

The combination of the basic principles provides a complete characterization of the critical flow properties at the weir crest with a rectangular cross section

$$d_{crest} = \sqrt[3]{\frac{\beta}{\Lambda} \times \frac{q^2}{g}} \tag{13}$$

$$V_{crest} = \sqrt[3]{\frac{\Lambda}{\beta} \times g \times q} \tag{14}$$

The water depth and velocity at the crest are related as

$$V_{crest} = \sqrt{\frac{\Lambda}{\beta} \times g \times d_{crest}} \tag{15}$$

and the minimum specific energy equals

$$E_{crest} = \frac{3}{2} \times \Lambda \times d_{crest} \tag{16}$$

The Bernoulli principle [Eq. (B-2)] yields the weir equation for an ideal fluid flow, neglecting friction and energy loss

$$Q = \sqrt{\frac{1}{\beta \times \Lambda^2}} \times \sqrt{g} \times \left(\frac{2}{3} \times (H_1 - \Delta z)\right)^{3/2} \times B \tag{17}$$

For an ideal fluid flow above the weir crest, C_D equals

$$C_D = \frac{1}{\sqrt{\beta \times \Lambda^2}} \quad \text{Ideal fluid flow} \tag{18}$$

The result is valid for any overflow weir shape. For an ideal fluid flow motion, the ratio $C_D/[1/(\beta \times \Lambda^2)]^{1/2}$ is unity. Experimental data (not shown) indicated some slight deviation from unity caused by friction and energy losses.

Appendix III. Pressure and velocity correction coefficient in critical flow above a broad crest with rounded edges (present study)

H_1 (m)	x/L	C_D	β	Λ	$\beta \times C_D^2 \times \Lambda^2$	$\Lambda \times d/(H_1 - \Delta z)$
0.110	0	1.036	1.016	0.928	0.940	0.777
0.110	0.185	0.970	1.011	1.005	0.961	0.694
0.110	0.369	0.953	1.012	1.011	0.939	0.625
0.110	0.554	0.953	1.013	0.999	0.919	0.599
0.110	0.738	0.917	1.015	1.000	0.853	0.563
0.110	0.923	0.939	1.015	0.879	0.691	0.439

Appendix III. (*Continued.*)

H_1 (m)	x/L	C_D	β	Λ	$\beta \times C_D^2 \times \Lambda^2$	$\Lambda \times d/(H_1 - \Delta z)$
0.110	1	0.996	1.025	0.384	0.150	0.164
0.151	0	0.985	1.022	0.928	0.855	0.789
0.149	0.185	0.983	1.008	1.000	0.975	0.730
0.149	0.369	0.967	1.009	1.007	0.956	0.644
0.150	0.554	0.970	1.010	1.000	0.951	0.595
0.149	0.738	0.981	1.010	0.963	0.901	0.541
0.150	0.923	0.985	1.012	0.820	0.659	0.403
0.150	1	1.035	1.025	0.289	0.092	0.123
0.200	0	1.026	1.028	0.920	0.916	0.798
0.200	0.185	1.004	1.007	0.988	0.990	0.761
0.200	0.369	1.010	1.007	1.014	1.057	0.701
0.200	0.554	0.995	1.007	1.002	1.001	0.625
0.200	0.738	1.014	1.007	0.991	1.017	0.563
0.200	0.923	0.988	1.009	0.805	0.639	0.387
0.200	1	1.036	1.021	0.565	0.349	0.239
0.235	0	1.018	1.034	0.928	0.923	0.804
0.235	0.185	1.032	1.007	0.978	1.025	0.768
0.235	0.369	1.010	1.014	0.994	1.021	0.699
0.235	0.554	1.012	1.015	0.991	1.021	0.631
0.235	0.738	1.006	1.012	0.962	0.948	0.548
0.235	0.923	1.039	1.016	0.492	0.265	0.243

Data Availability Statement

All data or models that support the findings of this study are available from the corresponding author upon reasonable request.

Acknowledgments

The authors acknowledge the technical assistance of Jason Van Der Gevel and Stewart Matthews (The University of Queensland). The financial support of the first author through the 2021-2022 UQ Summer Research Program is acknowledged.

Author Contributions

Sunhanut Chaokitka: Data curation; Investigation; Writing – review and editing. Hubert Chanson: Conceptualization; Formal analysis; Funding acquisition; Methodology; Project administration; Resources; Supervision; Visualization; Writing – original draft; Writing – review and editing.

Notation

The following symbols are used in this paper:

B = channel width (m), 0.985 m in the present study;
C_D = dimensionless discharge coefficient;
d = water depth (m);
d_c = critical flow depth (m);
g = gravity acceleration (m/s^2), $9.794 m/s^2$ in Brisbane, Australia;
H = total head (m);
H_1 = upstream total head (m);
L = broad-crest length (m), 0.542 m in the present study;
P = pressure (Pa);
P_w = wetted perimeter (m);
Q = water discharge (m^3/s);
q = water discharge per unit width (m^2/s): $q = Q/B$;
r = radius of curvature (m);
V = velocity (m/s);
V_x = longitudinal velocity component (m/s);
x = longitudinal distance (m) positive downstream;
y = vertical distance (m) measured perpendicular to and above the crest invert;
z = transverse distance (m) measured from the channel centerline;
z_o = invert elevation (m);
Δz = vertical weir height (m);
μ = dynamic viscosity (Pa·s) of water;
ρ = water density (kg/m^3);
τ_o = boundary shear stress (Pa);

Subscript

c = critical flow conditions;
crest = crest flow conditions; and
1 = upstream flow properties.

Supplemental Materials

Supplemental videos associated with this paper are available online in the ASCE Library (www.ascelibrary.org).

References

Ackers, P., W. R. White, J. A. Perkins, and A. J. M. Harrison. 1978. *Weirs and flumes for flow measurement*, 327. Chichester, UK: Wiley.

Bakhmeteff, B. A. 1912. "O Neravnomernom Dwijenii Jidkosti v Otkrytom Rusle." In *Varied flow in open channel*. [In Russian.] St Petersburg, Russia: Kubuch.

Bakhmeteff, B. A. 1932. "Hydraulics of Open." In *Channels*. 1st ed. New York: McGraw-Hill.

Bazin, H. 1896. "Expériences Nouvelles sur l'Ecoulement en Déversoir (5e article)." In Vol. 12 of *Annales des Ponts et Chaussées, Mémoires et Documents Relatif à l'Art des Constructions et au Service de l'Ingénieur*, 2nd ed. 645–731. Paris: Annales des Ponts et Chaussées.

Bélanger, J. B. 1841. "Notes sur l'Hydraulique." In *Ecole royale des ponts et chaussées*, 1841–1842. Paris: Ecole Royale des Ponts et Chaussées.

Bos, M. G. 1976. *Discharge measurement structures*. Publication No. 161, Delft, Netherlands: Delft Hydraulic Laboratory.

Cabonce, J., R. Fernando, H. Wang, and H. Chanson. 2019. "Using small triangular baffles to facilitate upstream fish passage in standard box culverts." *Environ. Fluid Mech.* 19 (1): 157–179. https://doi.org/10.1007/s10652-018-9604-x.

Castro-Orgaz, O., and H. Chanson. 2014. "Depth-averaged specific energy in open-channel flow and analytical solution for critical irrotational flow over weirs." *J. Irrig. Drain. Eng.* 140 (1): 04013006. https://doi.org/10.1061/(ASCE)IR.1943-4774.0000666.

Castro-Orgaz, O., and W. H. Hager. 2017. "Non-hydrostatic free surface flows." In *Advances in geophysical and environmental mechanics and Mathematics*, 696. Cham, Switzerland: Springer.

Chanson, H. 2004. *The hydraulics of open channel flow: An introduction*, 630. 2nd ed. Oxford, UK: Butterworth-Heinemann.

Chanson, H. 2006. Minimum specific energy and critical flow conditions in open channels. *J. Irrig. Drain. Eng.* 132 (5): 498–502. https://doi.org/10.1061/(ASCE)0733-9437(2006)132:5(498).

Felder, S., and H. Chanson. 2012. "Free-surface profiles, velocity and pressure distributions on a broad-crested weir: A physical study." *J. Irrig. Drain. Eng.* 138 (12): 1068–1074. https://doi.org/10.1061/(ASCE)IR.1943-4774.0000515.

Gonzalez, C. A., and H. Chanson. 2007. "Experimental measurements of velocity and pressure distribution on a large broad-crested weir."

Flow Meas. Instrum. 18 (3–4): 107–113. https://doi.org/10.1016/j.flowmeasinst.2007.05.005.

Govinda Rao, N. S., and D. Muralidhar. 1963. "Discharge characteristics of weirs of finite-crest width." *Houille Blanche* 49 (5): 537–545. https://doi.org/10.1051/lhb/1963036.

Henderson, F. M. 1966. *Open channel flow*. New York: MacMillan Company.

Isaacs, L. T. 1981. *Effects of laminar boundary layer on a model broad-crested weir*. Research Rep. No. CE28, Brisbane, Australia: Dept. of Civil Engineering, Univ. of Queensland.

Jaeger, C. 1956. *Engineering fluid mechanics*, 529. Glasgow, UK: Blackie & Son.

Liggett, J. A. 1993. "Critical depth, velocity profiles and averaging." *J. Irrig. Drain. Eng.* 119 (2): 416–422. https://doi.org/10.1061/(ASCE)0733-9437(1993)119:2(416).

Montes, J. S. 1998. *Hydraulics of open channel flow*, 697. Reston, VA: ASCE.

Ramamurthy, A. S., U. S. Tim, and M. V. J. Rao. 1988. "Characteristics of square-edged and round-nosed broad-crested weirs." *J. Irrig. Drain. Eng.* 114 (2): 61–73. https://doi.org/10.1061/(ASCE)0733-9437(1988)114:1(61).

Rouse, H. 1938. *Fluid mechanics for hydraulic engineers*, 422. New York: McGraw-Hill.

Tison, L. J. 1950. "Le Déversoir Epais." *J. La Houille Blanche* 36 (4): 426–439. https://doi.org/10.1051/lhb/1950045.

Wegmann, E. 1911. *The design and construction of dams*, 6th ed. New York: Wiley.

Woodburn, J. G. 1932. "Tests of broad-crested weirs." *Transactions* 96 (1): 387–416.

Zhang, G., and H. Chanson. 2015. "Broad-crested weir operation upstream of a steep stepped spillway." In *Proc., 36th IAHR World Congress*, 2901–2911. Madrid, Spain: CEDEX.

Zhang, G., and H. Chanson. 2016. "Hydraulics of the developing flow region of stepped spillways. I: Physical modeling and boundary layer development." *J. Hydraul. Eng.* 142 (7): 8. https://doi.org/10.1061/(ASCE)HY.1943-7900.0001138.

Erratum for "Hydrodynamics of a Broad-Crested Weir with Rounded Edges"

Sunhanut Chaokitka

Researcher, School of Civil Engineering, Univ. of Queensland, Brisbane, QLD 4072, Australia; presently, Structural Engineer, Aurecon, Brisbane, QLD 4006, Australia. ORCID: https://orcid.org/0009-0000-8988-2430

Hubert Chanson

Professor in Hydraulic Engineering, School of Civil Engineering, Univ. of Queensland, Brisbane, QLD 4072, Australia (corresponding author). ORCID: https://orcid.org/0000-0002-2016-9650. Email: h.chanson@uq.edu.au

The following correction should be made to "Hydrodynamics of a Broad-Crested Weir with Rounded Edges" by Sunhanut Chaokitka and Hubert Chanson (https://doi.org/10.1061/JIDEDH.IRENG-10666):

The authors discovered typographical errors in Fig. 1(b) and Eq. (4) in the original manuscript. These errors do not affect the data or change any results or conclusions. The corrected figure and equation are provided herein

$$C_D = 0.90 + 0.26 \times \frac{H_1 - \Delta z}{L} \quad \text{for } 0.2 < \frac{H_1 - \Delta z}{L} < 0.45 \qquad (4)$$

The authors regret the errors. To preserve the published version of record, these details have been corrected only in this erratum.

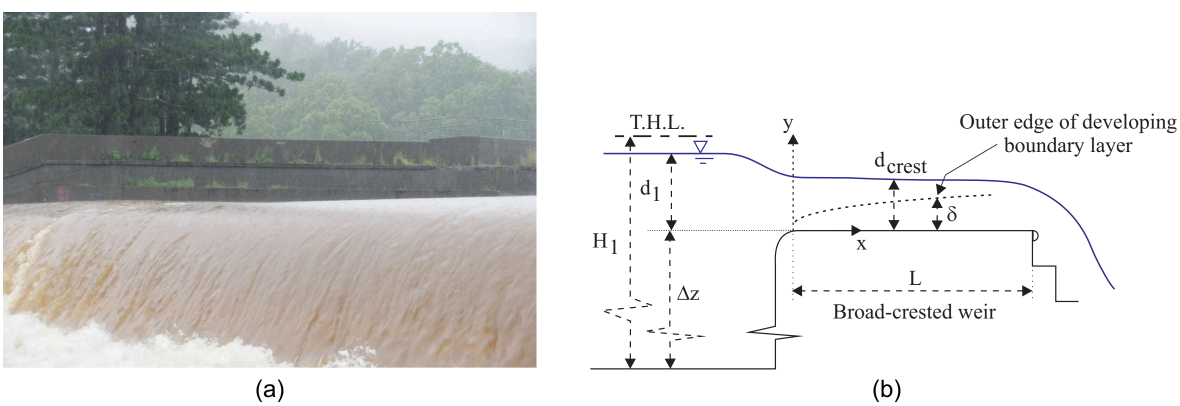

Fig. 1. Flow with a broad crest: (a) Gold Creek Dam spillway (Australia) in operation on February 26, 2022, for $Q = 38\ m^3/s$; and (b) definition sketch of an overflow above a broad crest with rounded edge.